

1. **Studies of signal and background separation using Mann-Whitney U test and some new methods**

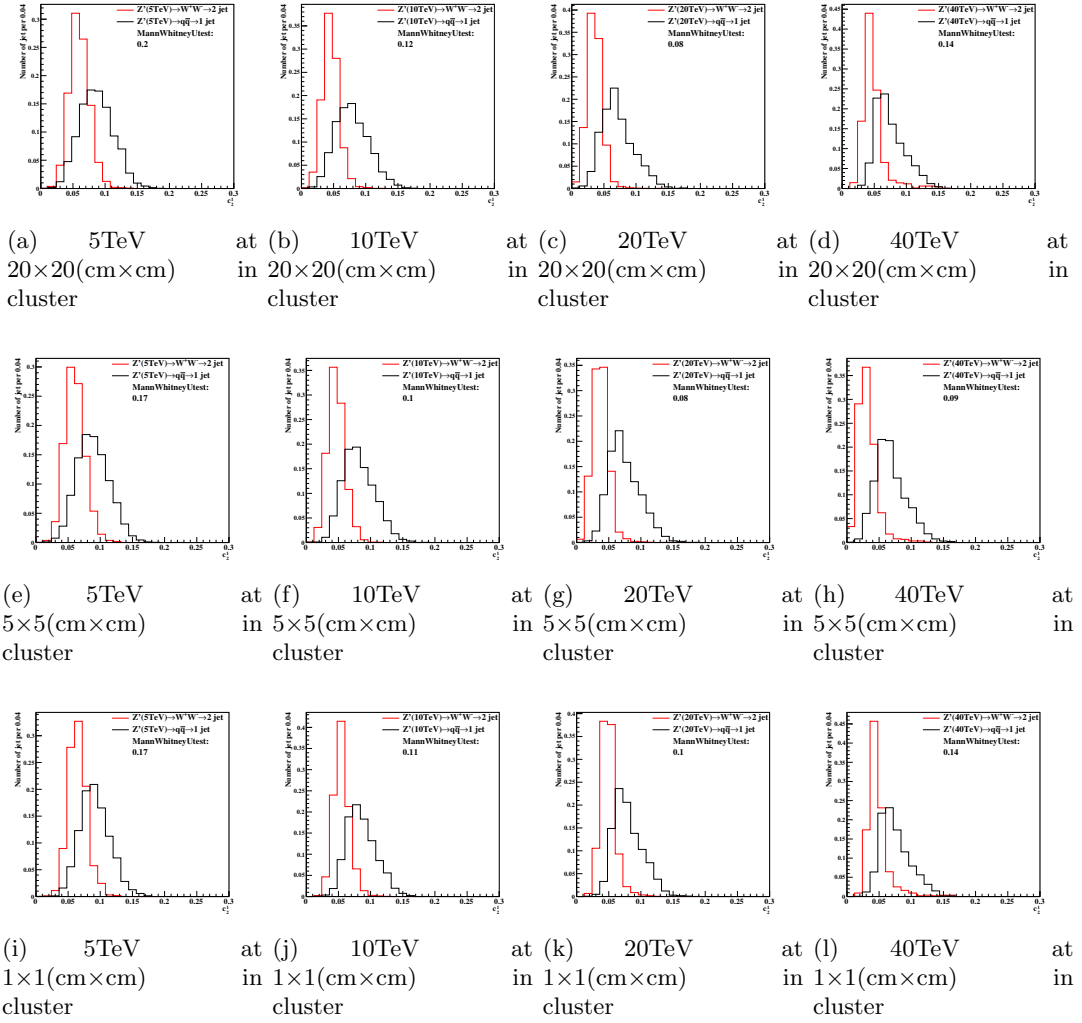
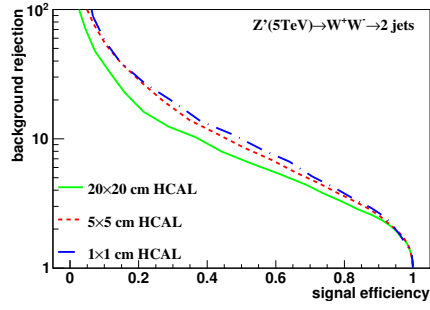
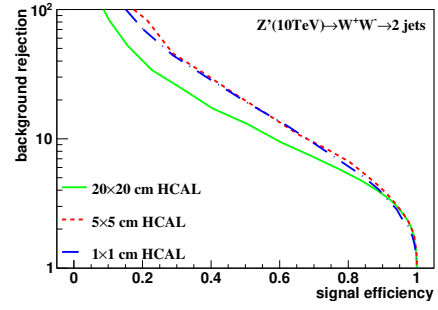


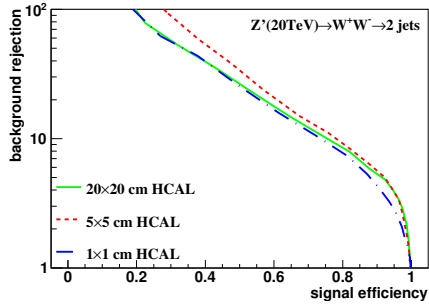
Figure 1: Distributions of Mann-Whitney value  $U$  in 5, 10, 20, 40 TeV energy collision for  $c_2^{(1)}$  in different detector sizes. Cell Size in  $20 \times 20$ ,  $5 \times 5$ , and  $1 \times 1(\text{cm} \times \text{cm})$  are shown here.



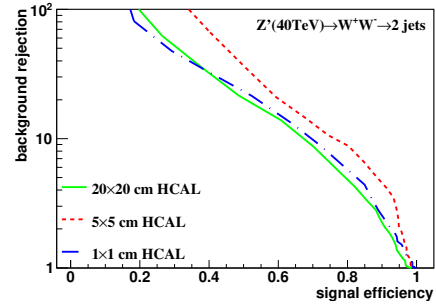
(a) 5 TeV in cluster



(b) 10 TeV in cluster



(c) 20 TeV in cluster



(d) 40 TeV in cluster

Figure 2: Signal efficiency versus background rejection rate using  $c_2^{(1)}$ . The energies of collision at (a)5, (b)10, (c)20, (d)40TeV are shown here. In each picture, the three ROC curves correspond to different detector sizes.

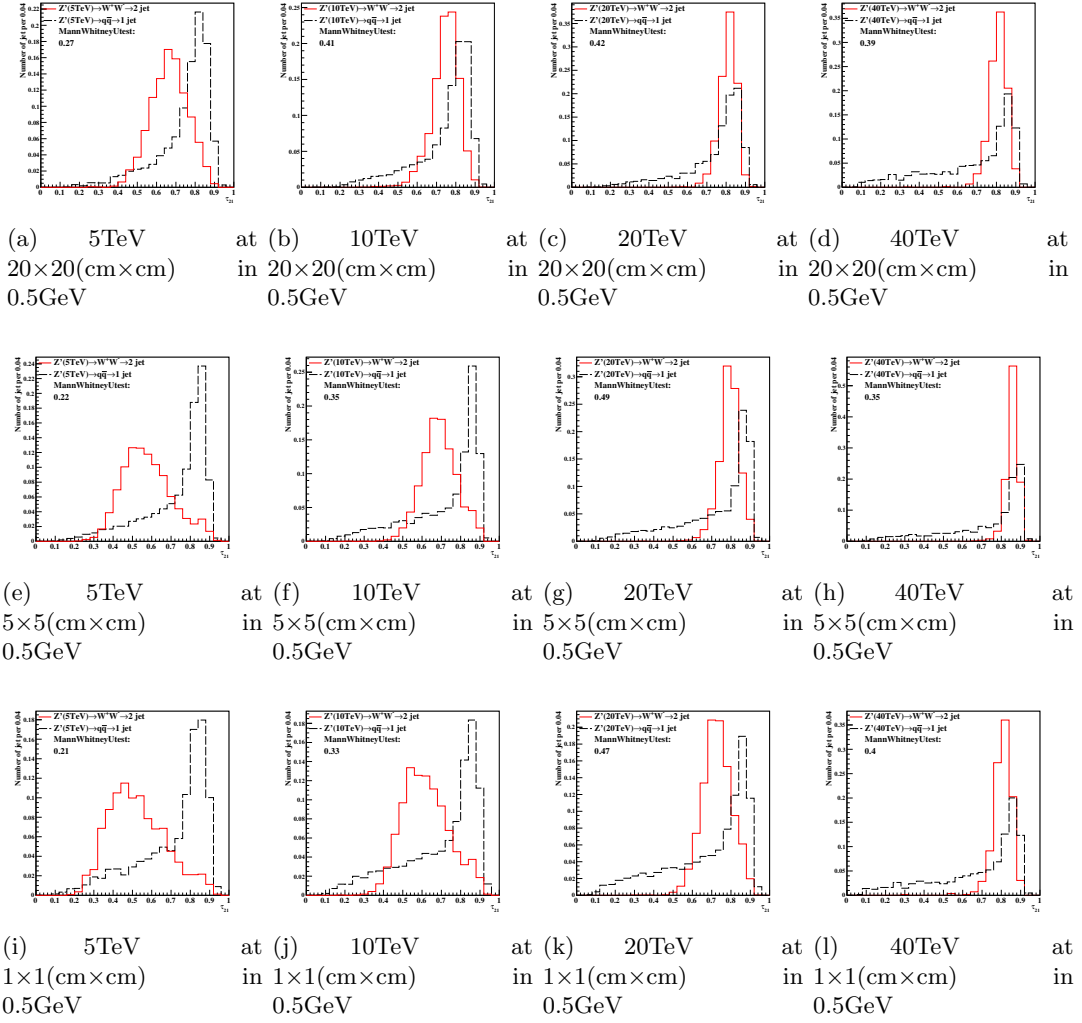
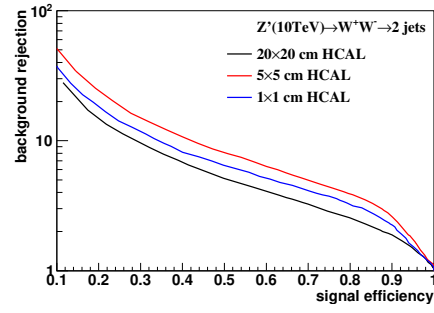
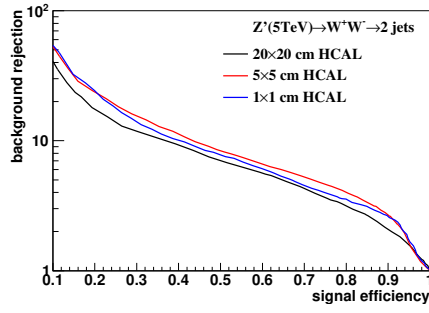
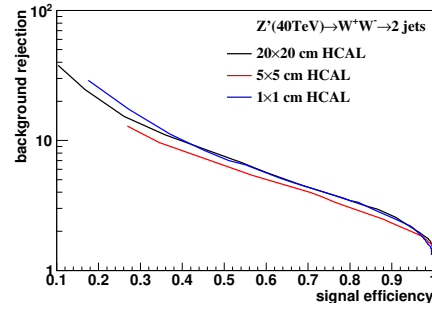
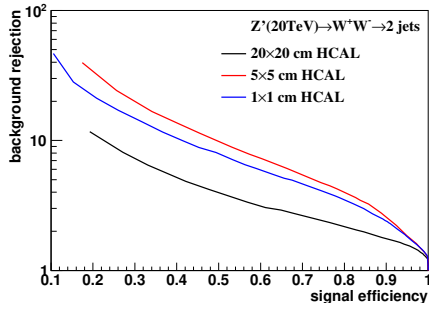


Figure 3: Distributions of Mann-Whitney value U in 5, 10, 20, 40TeV energy collision for  $\tau_{21}$  in different detector sizes. Cell Size in 20x20, 5x5, and 1x1(cm x cm) are shown here.



(a) 5 TeV rawhit cut at 0.5GeV compare with New2 Method (b) 10 TeV rawhit cut at 0.5GeV compare with New2 Method



(c) 20 TeV rawhit cut at 0.5GeV compare with New2 Method (d) 40 TeV rawhit cut at 0.5GeV compare with New2 Method

Figure 4: Signal efficiency versus background rejection rate using  $\tau_{21}$ . The energies of collision at (a)5, (b)10, (c)20, (d)40TeV are shown here. In each picture, the three ROC curves correspond to different detector sizes.

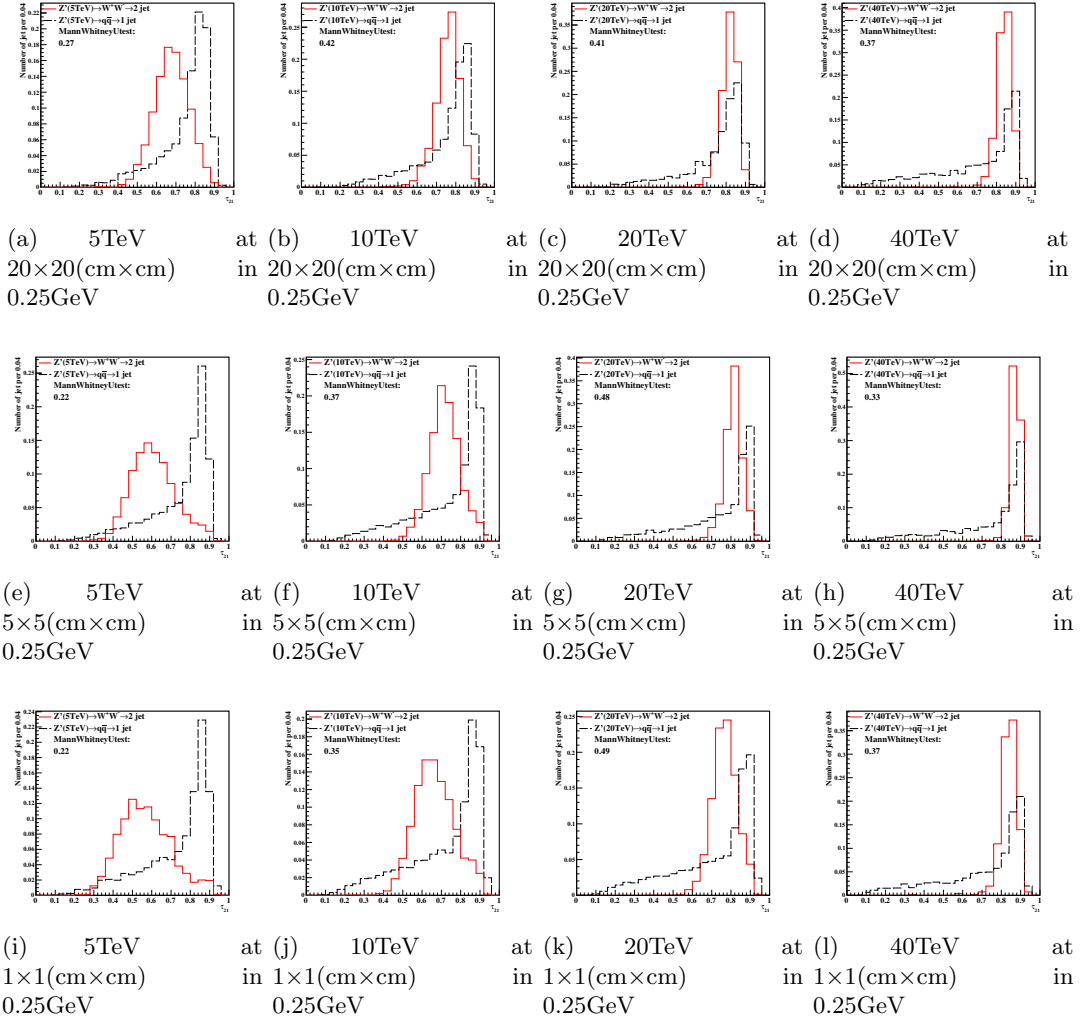
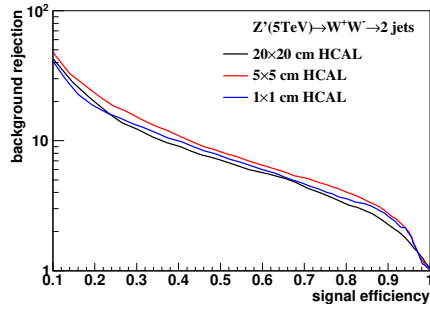
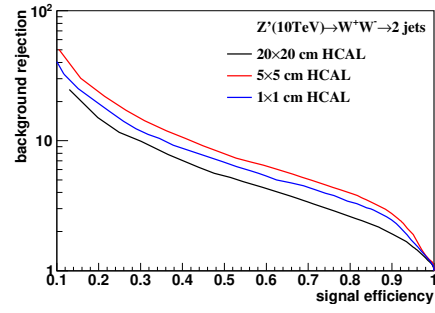


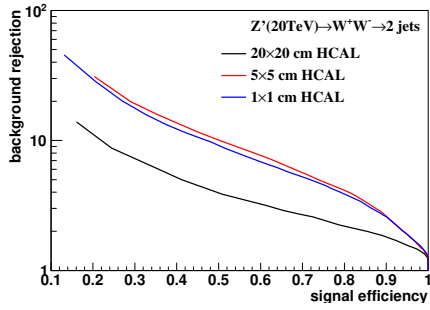
Figure 5: Distributions of Mann-Whitney value U in 5, 10, 20, 40TeV energy collision for  $\tau_{21}$  in different detector sizes. Cell Size in 20x20, 5x5, and 1x1(cm×cm) are shown here.



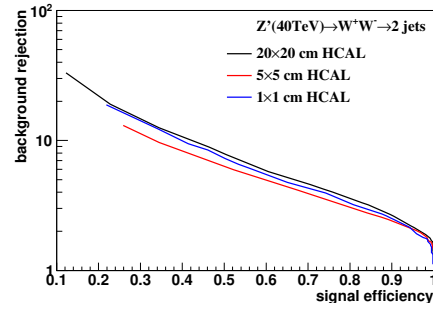
(a) 5 TeV rawhit cut at 0.25GeV compare with New2 Method



(b) 10 TeV rawhit cut at 0.25GeV compare with New2 Method



(c) 20 TeV rawhit cut at 0.25GeV compare with New2 Method



(d) 40 TeV rawhit cut at 0.25GeV compare with New2 Method

Figure 6: Signal efficiency versus background rejection rate using  $\tau_{21}$ . The energies of collision at (a)5, (b)10, (c)20, (d)40TeV are shown here. In each picture, the three ROC curves correspond to different detector sizes.

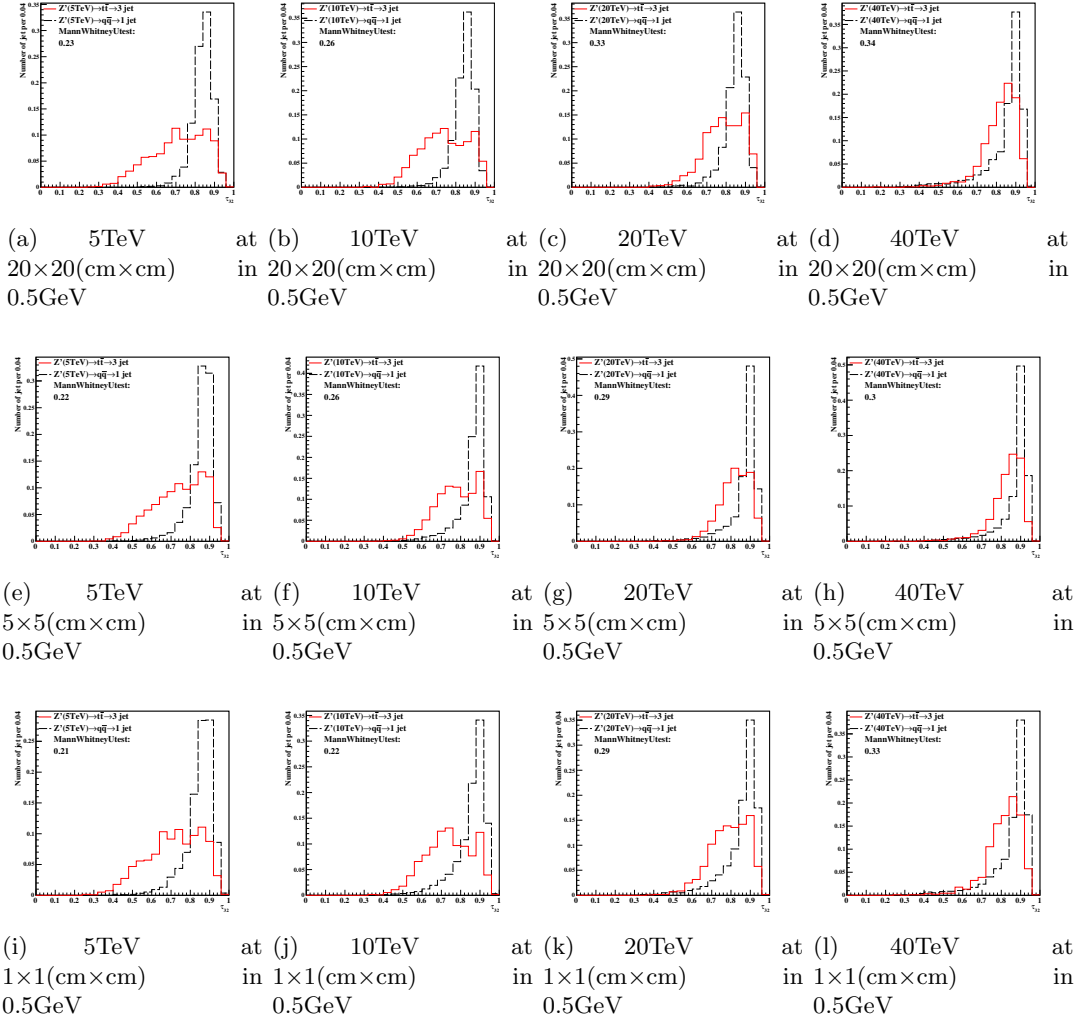
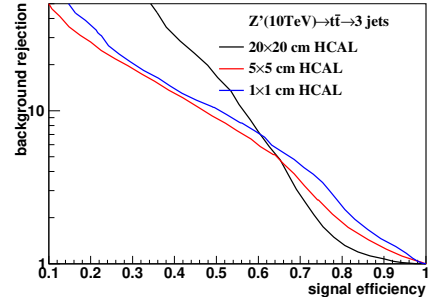
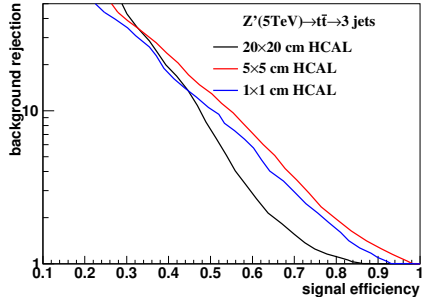
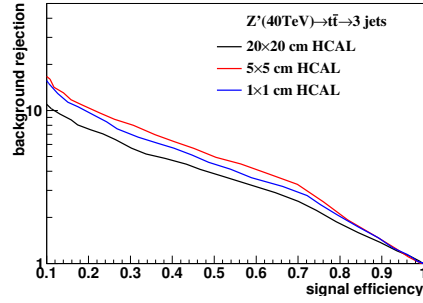
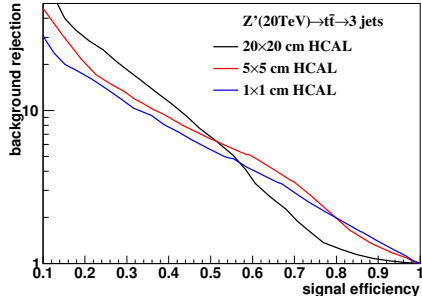


Figure 7: Distributions of Mann-Whitney value U in 5, 10, 20, 40 TeV energy collision for  $\tau_{32}$  in different detector sizes. Cell Size in 20×20, 5×5, and 1×1(cm×cm) are shown here.





(a) 5 TeV rawhit cut at 0.5GeV compare with New2 Method (b) 10 TeV rawhit cut at 0.5GeV compare with New2 Method



(c) 20 TeV rawhit cut at 0.5GeV compare with New2 Method (d) 40 TeV rawhit cut at 0.5GeV compare with New2 Method

Figure 8: Signal efficiency versus background rejection rate using  $\tau_{32}$ . The energies of collision at (a)5, (b)10, (c)20, (d)40TeV are shown here. In each picture, the three ROC curves correspond to different detector sizes.

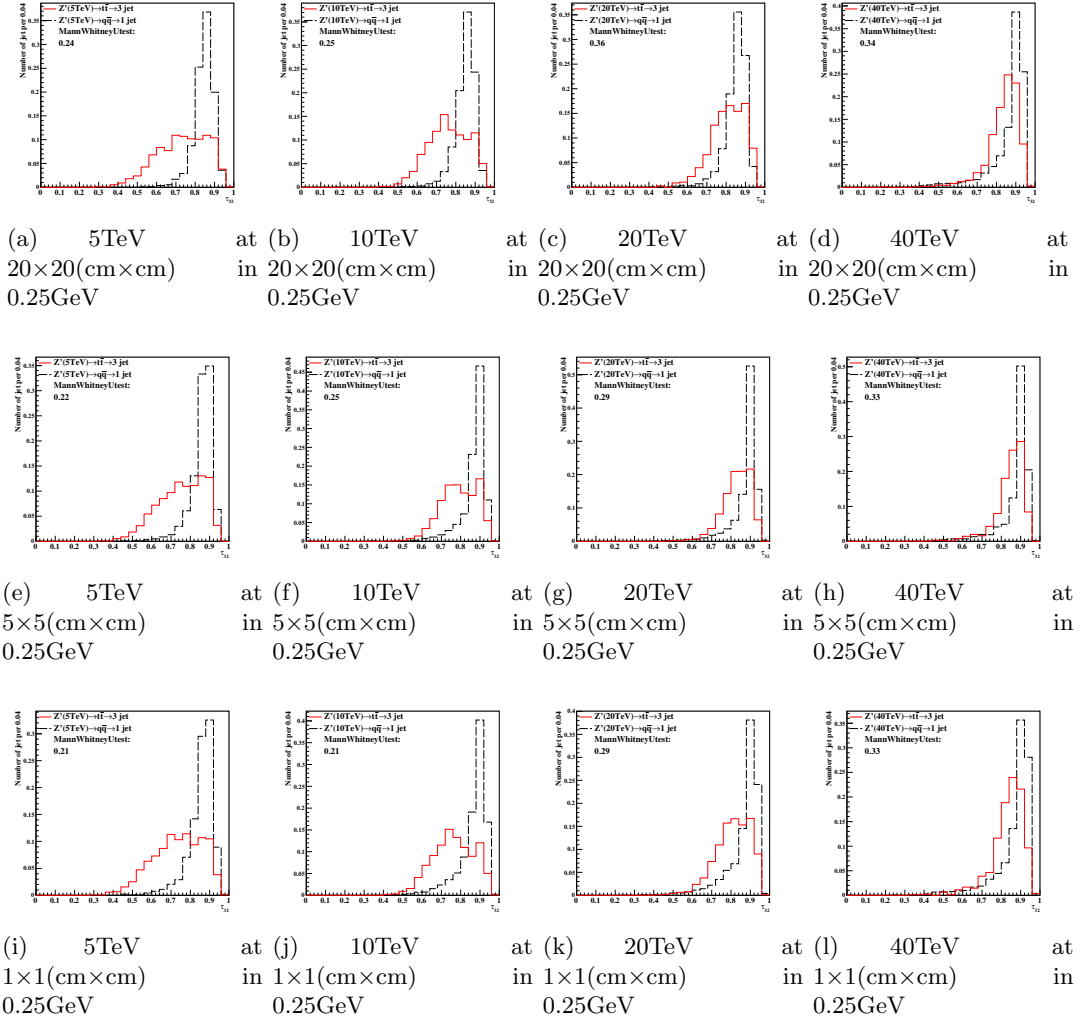
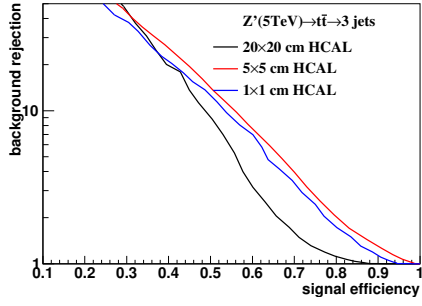
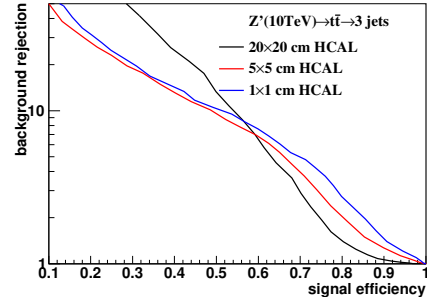


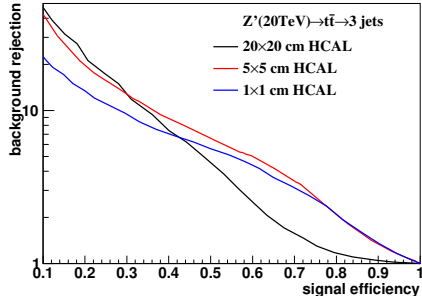
Figure 9: Distributions of Mann-Whitney value  $U$  in 5, 10, 20, 40 TeV energy collision for  $\tau_{32}$  in different detector sizes. Cell Size in 20×20, 5×5, and 1×1(cm×cm) are shown here.



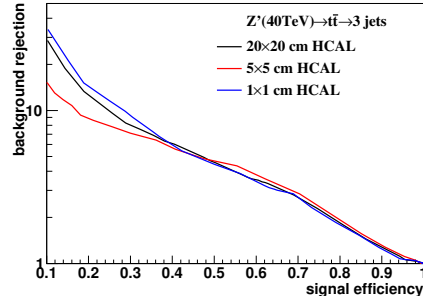
(a) 5 TeV rawhit cut at 0.25GeV compare with New2



(b) 10 TeV rawhit cut at 0.25GeV compare with New2

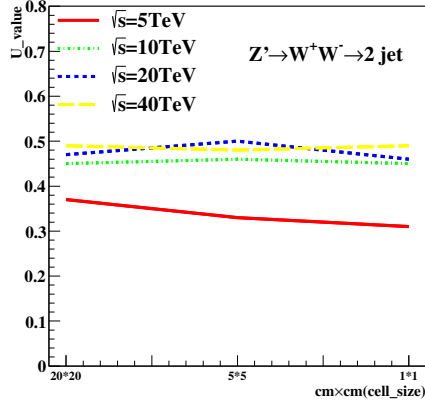


(c) 20 TeV rawhit cut at 0.25GeV compare with New2

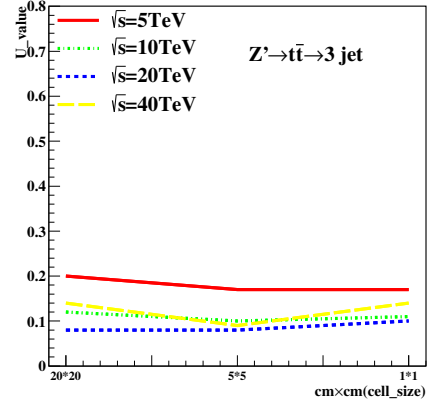


(d) 40 TeV rawhit cut at 0.25GeV compare with New2

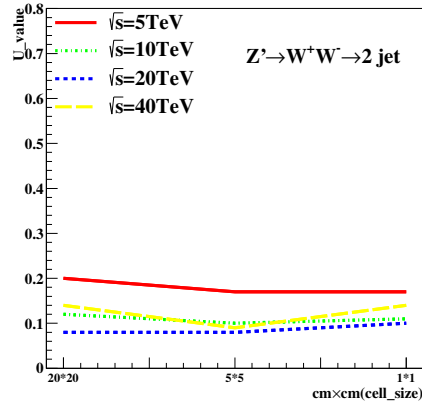
Figure 10: Signal efficiency versus background rejection rate using  $\tau_{32}$ . The energies of collision at (a) 5, (b) 10, (c) 20, (d) 40 TeV are shown here. In each picture, the three ROC curves correspond to different detector sizes.



(a)  $\tau_{21}$  in cluster

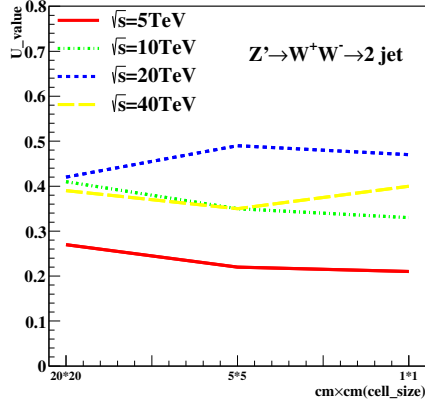


(b)  $\tau_{32}$  in cluster

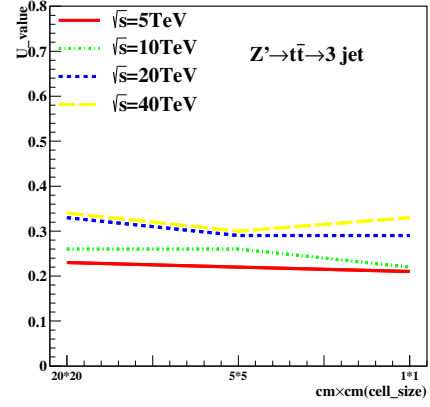


(c)  $c_2^{(1)}$  in cluster

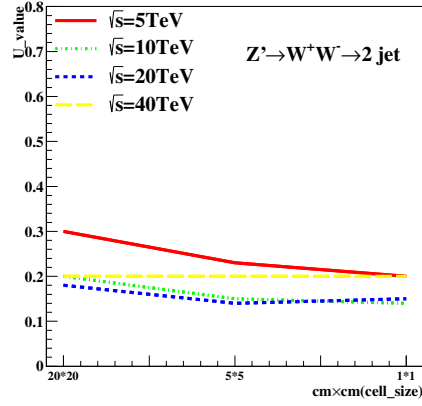
Figure 11: The Mann-Whitney U values for  $\tau_{21}, \tau_{32}$  and  $c_2^{(1)}$  reconstructed from calorimeter clusters at different collision energies correspond to different detector sizes in cluster. The energies of collision at 5, 10, 20, 40, 20, 40 TeV are shown in each figure.



(a)  $\tau_{21}$  rawhit cut at 0.5 GeV

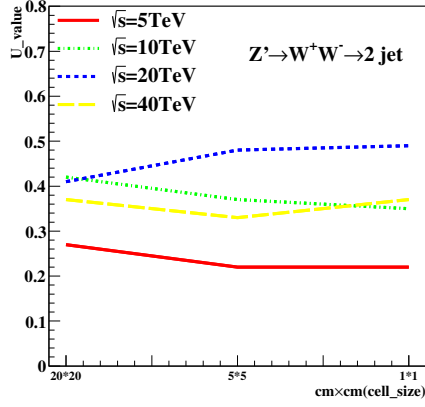


(b)  $\tau_{32}$  rawhit cut at 0.5 GeV

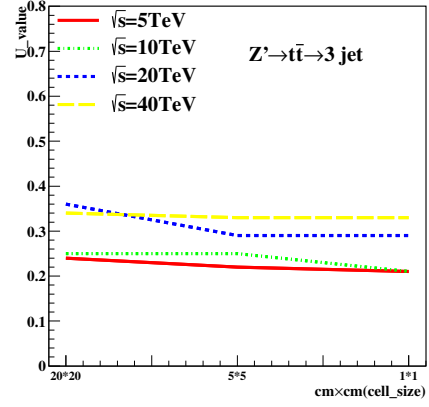


(c)  $c_2^{(1)}$  rawhit cut at 0.5 GeV

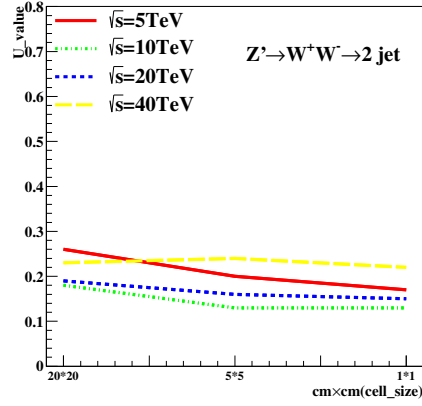
Figure 12: The Mann-Whitney U values for  $\tau_{21}, \tau_{32}$  and  $c_2^{(1)}$  reconstructed from calorimeter hit at 0.5 GeV cut at different collision energies correspond to different detector sizes in rawhit cut at 0.5 GeV. The energies of collision at 5, 10, 20, 40, 20, 40 TeV are shown in each figure.



(a)  $\tau_{21}$  rawhit cut at 0.25GeV



(b)  $\tau_{32}$  rawhit cut at 0.25GeV



(c)  $c_2^{(1)}$  rawhit cut at 0.25GeV

Figure 13: The Mann-Whitney U values for  $\tau_{21}, \tau_{32}$  and  $c_2^{(1)}$  reconstructed from calorimeter hit at 0.25GeV cut at different collision energies correspond to different detector sizes in cluster. The energies of collision at 5, 10, 20, 40, 20, 40TeV are shown in each figure.